Hindawi
Mathematical Problems in Engineering
Volume 2019, Article ID 4302851, 13 pages
https://doi.org/10.1155/2019/4302851

Research Article

Outer Rotor Permanent Magnet Passively Compensated Pulsed Alternator for Electromagnetic Railgun System

Yaqian Chen,[1] **Bingyi Zhang**,[1] **Shuai Wang**,[1,2] **Haoyu Zhang**,[2] **and Guihong Feng**[1]

[1]*School of Electrical Engineering, Shenyang University of Technology, Shenyang 110870, China*
[2]*School of Materials Science and Engineering, Shenyang University of Technology, Shenyang 110870, China*

Correspondence should be addressed to Yaqian Chen; 964922601@qq.com

Received 26 September 2019; Revised 25 November 2019; Accepted 3 December 2019; Published 21 December 2019

Academic Editor: Salvatore Alfonzetti

In the compensated pulsed alternator, the slotless armature winding and internal rotor structure with electric excitation are usually adopted. The above structure can effectively reduce the air gap leakage and has the simple structure, but it exhibits such disadvantages that the armature winding is difficult to disperse the heat and to be fixed, the shielding element is easy to deform due to the centrifugal force in the discharge process, and both reversing device and energy storage flywheel need to be used. In this investigation, an outer rotor permanent magnet passively compensated pulsed alternator was designed to solve the above problems. Then, a collaborative simulation model for the railgun system driven by outer rotor permanent magnet passively compensated pulsed alternator was built with the ANSYS simulation platform. The no-load characteristics of the alternator, the output characteristics of the alternator, and the performances of the railgun system were compared and analyzed under three kinds of pole and slot matching. The present research can provide the theoretical foundation and reference for the further engineering application of an outer rotor permanent magnet passively compensated pulsed alternator.

1. Introduction

The transformation in the launching mode from the mechanical energy to the chemical energy had been realized with the development from the bow and arrow to the artillery. The electromagnetic launch has a higher speed and will be an inevitable trend from the chemical energy launch to electromagnetic energy launch in the future. The power supply for driving the electromagnetic railgun system needs to be the pulsed power supply, which is to store slowly the energy in some form and then quickly output the large electric energy to the electromagnetic railgun as the load within a very short time [1, 2]. As one of core components in the electromagnetic railgun system, the performance of pulsed power supply will obviously affect the whole electromagnetic launch system. At present, the typical challenge in the development and application of electromagnetic railgun is how to realize high output power and high-frequency discharge as well as the miniaturization of pulsed power supply [3–6]. The pulse power supply to realize the energy storage with the capacitor usually has the large volume, its energy storage density and discharge frequency are low, and additionally the charging device and high power circuit switch are required. The energy storage density of an inductor is higher than that of a capacitor. However, the high power circuit switch is also required, and the technology is immature at present. The energy storage density of battery is very high, but due to the limitation of chemical reaction speed, the time of energy storage and release is very long, and the power density is very low. In addition, the internal resistance of traditional generator is large so that it is difficult to obtain the pulse with both narrow width and high amplitude required by the load. The compensated pulsed alternator (CPA) is a new type of pulsed power supply and concentrates such functions as the inertial energy storage, electromechanical energy conversion, and pulse forming in one device. The CPA with such advantages as the high power density, high pulse discharge frequency, and easy waveform adjustment is also the preferred power source for engineering electromagnetic launching systems in the future [7]. The difference between the CPA and conventional generators is that the CPA works at the transient state and the

magnetic flux in the air gap is compressed with a special compensating unit to reduce the inductance of armature winding, and thus a high pulse current whose peak is more than tens or even hundreds of kiloamperes can be generated instantaneously within 20 μs to 10 ms [8–10].

The compensation methods for the CPA mainly include such three types as the active compensation, passive compensation, and passive selective compensation, and the compensation forms can be selected according to the requirement on the load waveform [11–13]. At present, the slotless armature which is attached to the stator surface is usually adopted for most of the CPAs, and thus the leakage reactance of stator slot and the leakage reactance at the tip of tooth can be eliminated to reduce the air gap leakage inductance. However, the effective dissipation of heat for the windings is difficult, the displacement is easy to generate under the action of impact force during the discharge, and the equivalent air gap length will also increase [14–16]. The simple internal rotor structure is often used in the CPA. Due to the higher speed of CPA which can reach to more than 10000 rpm, the compensating unit positioned outside the inner rotor is easy to deform under the centrifugal force generated with the high-speed rotation of rotor, which will bring the vibration and noise, even cause the contact fault between the air gap of stator and rotor, and lead to the damage of the CPA. In addition, the internal rotor structure usually needs an additional flywheel to increase the energy density [17, 18]. The electric excitation mode is adopted for most of the CPAs, where the excitation magnetic field is generated by the current in the excitation winding. Thus, the large copper loss will occur, and the commutator and sliding ring are easy to damage. With the electric excitation, the efficiency of CPA is reduced, and the safe and stable operation of CPA is not favorable [19–21].

In this investigation, an outer rotor permanent magnet passively compensated pulsed alternator (ORPMPCPA) has been designed. The outer rotor structure and the passive compensation mode are adopted in the CPA, and the shielding cylinder is placed at the inside of the rotor. Thus, the shielding cylinder is subjected to the compressive stress under the influence of centrifugal force, and the mechanical strength of rotor can get increased. In addition, the flywheel is replaced by the outer rotor with the greater rotation inertia to store the mechanical energy. The excitation magnetic field of ORPMPCPA is produced by the permanent magnet with the built-in tangential structure instead of the electric current. Thus, the magnetic field energy is larger, the mechanical strength is higher, and the operation efficiency and system reliability are improved. The two-phase orthogonal winding is placed in the stator core groove, the equivalent air gap length is reduced, the force acting on the winding is dispersed along the radial direction, and the shock resistance of the CPA is improved. On the basis of the design scheme, the time-varying load parameters of the railgun system are calculated. Based on the finite element analysis platform ANSYS with the strong collaborative function, a cooperative simulation model for both the ORPMPCPA and gun system driven by the CPA is established under three kinds of pole and slot matching. In addition, the no-load and short-circuit output characteristics of the ORPMPCPA as well as the performances of the railgun system in three cases are compared and analyzed.

2. Design for ORPMPCPA

The CPA is essentially a synchronous generator which compresses the air gap flux to change the transient inductance of winding. It is obvious that the transient inductance value of winding directly affects the output pulse current of CPA. If the load needs to obtain a larger power in a short time, the armature winding with very small inductance and resistance must be designed. Because the inductance of armature winding is proportional to the square of winding turns for the alternator and is inversely proportional to the reluctance in the magnetic circuit of alternator, it is necessary to reduce the number of turns and increase the magnetic resistance for reducing the inductance. Thus, a shielding cylinder with the electric-conducting and conducting magnetic-insulating function is sheathed on the rotor surface of the ORPMPCPA, where the passive compensation mode can be realized. When the armature winding is discharging for the load, the response magnetic field of armature will induce the eddy current equal to its ampere turns, the eddy current magnetic field is opposite to the armature reaction field, and the armature response flux is compressed into the air gap between the shielding cylinder and armature winding. Thus, the magnetic circuit length increases, the permeance decreases, and the winding transient inductance of CPA get greatly reduced during the discharge. Moreover, the compensating action of shielding cylinder is symmetrical on the whole circumference, and the waveform of output pulse current is approximately sinusoidal wave.

Because the CPA works in the instantaneous short-circuit state, the short-time pulse power is very large, the dissipating time of heat is long, and the heat load can reach a high value. Therefore, the size of the CPA cannot be determined according to the rated power which is usually used for determining the size of conventional motor, and the main size of the CPA should be determined from the view of inertia energy storage. Actually, the rotor of the ORPMPCPA can be regarded as the cylinder structure, and thus the calculating formula for the inertia energy storage of rotor, E_r, can be expressed as follows:

$$E_r = \frac{\pi}{4}\rho_r \beta\left(1-\lambda^4\right) b_r^3 v_{tip}^2, \tag{1}$$

where ρ_r is the average mass density of rotor which may be estimated according to the materials used for each component, β is the length to diameter ratio of rotor, λ is the ratio of inner diameter to outer diameter of rotor, b_r is the outer radius of rotor, and v_{tip} is the linear velocity at the rotor edge. In the equation (1), several variables may change in a certain range to meet the energy storage requirement of rotor and then can be used for determining the main size of the CPA.

Because the CPA is a pulsed working system, the electromagnetic load cannot be determined according to the conventional formula and experience. For the selection of

magnetic load, it should be considered to maximize the effective magnetic energy provided by the permanent magnet to the external magnetic circuit. The magnetic load should be increased as much as possible within the allowable range of rotor excitation capacity, to reduce the size of motor and to increase the power density and energy density. Because the pulse current with great amplitude flows through the armature winding, the selection of for the electric load of CPA is different from that for the ordinary alternator. However, the electric load can be selected and calibrated through calculating the heat capacity of conductor in the short-term heat-releasing state. The calculating principle is as follows. The temperature rise of motor winding under a certain working system is lower than the maximum temperature limited by the insulation level of winding. If the heat generated by the current flowing through the conductor converts into the temperature rise of winding rather than transfer outward at the moment of discharge, the allowable cross-sectional area of conductor, S, can be calculated according to the extreme temperature rise of winding and the heat capacity generated inside the conductor, as given in the following equation:

$$S = \sqrt{\frac{I_s^2 t_k \rho_0 \alpha}{\gamma c \ln\left(1 + \alpha\theta_k / 1 + \alpha\theta_0\right)}}, \tag{2}$$

where the I_s is the short-circuit current, ρ_0 is the resistivity of winding at 0°C, θ_0 is the temperature of conductor before being electrified, θ_k is the maximum allowable heating temperature of conductor after being electrified, γ is the density of conductor, c is the specific heat capacity of conductor, α is the resistance temperature coefficient of conductor, and t_k is the heating time. For the ORPMPCPA, the material of stator winding is copper, and thus ρ_0 is $1.678 \times 10^{-8}\ \Omega$·m, γ is 8900 kg/m^3, c is 390 J/(kg·°C), and α is 0.00393. When I_s is 180 kA, θ_0 is 20°C, θ_k is 100°C, and t_k is 2.5 ms, the calculated value of S should be 245.19 mm^2. Considering the actual working condition of the generator, the additional area margin should be reserved, and thus the value of S is taken as 300 mm^2.

The usage of conductive shielding cylinder is a key problem in the design of CPA and is also one of main differences between the CPA and conventional generator [22–24]. Because the shielding cylinder material is nonmagnetic, its thickness corresponds to a part of air gap. In order to achieve the ideal compensation effect, the shielding cylinder should usually possess the larger thickness. However, much larger thickness will lead to the increase of air gap, and the excitation magnetic potential and magnetic loss will increase. Generally, the appropriate thickness of shielding cylinder is selected according to the penetration depth of magnetic field. The expression for the penetration depth of magnetic field, δ, is as follows:

$$\delta = \sqrt{\frac{1}{\pi f \mu \gamma}}, \tag{3}$$

where f is the rated frequency, μ is the magnetic permeability of conductor, and γ is the electric conductivity of conductor. Considering the conductivity and mechanical strength of nonmagnetic material, the aluminum is selected as the material for the shielding cylinder. For the aluminum, μ is $4\pi \times 10^{-7}$ H/m and γ is 3.82×10^7 S/m. When f is 400 Hz, the value of δ is determined as 4.072 mm. Synthetically considering the effect of magnetic flux compression, processing technology, and mechanical strength, the thickness of shielding cylinder is selected as 6 mm.

The air gap size has a great influence on the performances as well as the manufacturing and assembly of motor. If the air gap is large, the magnetic resistance of excitation magnetic circuit is large, and the thickness of permanent magnet needs to be greatly increased. However, when the air gap is large, the machining accuracy of relevant parts may be properly reduced, and the assembly difficulty gets decreased. In the actual selection, the determination of air gap size is closely related with the slenderness ratio and inner diameter of motor. The CPA is different from the conventional generator, and its air gap includes the thickness of shielding cylinder, which is usually large. In the selection, all influencing factors should be comprehensively taken into account, and the air gap should be selected as small as possible.

The main parameters of ORPMPCPA are shown in Table 1.

In the ORPMPCPA, an outer rotor structure with a built-in tangential magnetic pole is adopted, and the tangential magnetic pole is placed inside the outer rotor. Obviously, the influence of centrifugal force on the magnetic pole can be effectively overcome when rotor is rotating at high speed, the air gap magnetic flux density gets increased, and the output capacity of CPA is enhanced. At the same time, because the shielding cylinder is fixed on the inner surface of rotor, the shielding cylinder is subjected to the compressive stress under the influence of centrifugal force, and the mechanical strength of rotor gets increased. Obviously, the contact fault between the air gap of stator and rotor, which is caused by the deformation of shielding cylinder under the action of centrifugal force when the inner rotor rotates at high speed, can be avoided. In addition, the outer rotor structure can also greatly improve the rotating inertia and energy storage density of the CPA.

The inductance of generator is usually composed of self-inductance and mutual inductance. In order to reduce the mutual inductance between the windings, two-phase symmetrical winding with 90 degrees of electrical angle difference is adopted, and the electrical decoupling is realized. The independence of two-phase windings with each other is beneficial to increase the output pulse width and modulate the waveform of output current. Because the single-layer concentric winding can shorten the length of armature winding wire and reduce the inductance and resistance of armature winding, the single-layer concentric winding structure is used in the alternator winding. At the same time, the number of parallel branches is increased to reduce further the internal impedance of winding. The overall structure of ORPMPCPA is illustrated in Figure 1. The layout of armature winding for the ORPMPCPA is illustrated in Figure 2.

Table 1: Main parameters of ORPMPCPA.

Peak power (GW)	2.5
Rotation inertia (kg·m^2)	7000
Rotation speed of alternator (rpm)	12000
Outer diameter of stator (mm)	1180
Outer diameter of rotor (mm)	1860
Core length (mm)	700
Air gap (mm)	1
Thickness of compensating cylinder (mm)	6
Section area of winding (mm^2)	300
Air gap flux density (B_δ/T)	0.98
Phase number of winding	2
Number of parallel branches	4
Number of conductors per slot	2
Number of poles	4

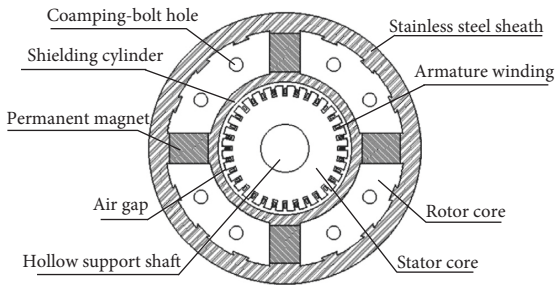

Figure 1: Overall structure diagram of ORPMPCPA.

As a new type of pulsed power supply, the CPA needs to provide enough power for driving the high-technical equipment in a certain space. The output power of CPA is mainly determined by its output voltage and internal impedance. Actually, the basic electromagnetic law is still conformable to the CPA. The output voltage of CPA is the same as that of conventional generator and can be expressed as follows:

$$U = U_m \sin(2\pi f t + \theta), \tag{4}$$

where U_m is the terminal voltage amplitude of the CPA, f is the frequency of the CPA, and θ is the initial phase angle of voltage when the external circuit is connected, which is also the trigger angle of the CPA. Because the discharge process of the CPA is the zero state response process of first-order circuit, the driving load current of the CPA after the switch being closed can be written as follows:

$$i = \frac{U_m}{\sqrt{R^2 + (2\pi f L)^2}} \cos(2\pi f t) - \frac{U_m}{\sqrt{R^2 + (2\pi f L)^2}} e^{-(Rt/L)}. \tag{5}$$

Thus, the output power of the CPA can be calculated with the following formula:

$$P = iU = \frac{U_m^2}{\sqrt{R^2 + (2\pi f L)^2}} \sin(2\pi f t + \theta)\cos(2\pi f t) - \frac{U_m^2}{\sqrt{R^2 + (2\pi f L)^2}} \sin(2\pi f t + \theta) e^{-(Rt/L)}, \tag{6}$$

where R and L are the total equivalent resistance and inductance in the discharge circuit. In fact, $R = R_a + R_b$ and $L = L_a + L_b$, where R_a and L_a are the internal resistance and inductance of the CPA while R_b and L_b are the resistance and inductance of load. It can be seen from the equation (6) that the output power of the CPA is related to the output voltage of the CPA and the impedance in the discharge circuit. Since the load impedance in the discharge circuit has been fixed during the design, the output power of the CPA is mainly dependent on the output voltage and internal impedance of the CPA. Obviously, both output voltage and internal impedance of the CPA should be considered in the design of the CPA, in order to achieve the output power needed to drive the load.

Three different combinations of pole and groove are compared and analyzed when the number of slots per phase and per pole q is equal to 2, 4, and 6, and its effect on the output power of the ORPMPCPA is investigated to obtain a more appropriate scheme. In the comparative analysis concerning different q values, such structural dimensions as the internal and external diameter of both stator and rotor and the length of core as well as such electrical parameters as the number of conductors per slot and the number of parallel branches are kept unchanged.

3. Simulation of No-Load Characteristics and Calculation of Load Impedance for ORPMPCPA

3.1. Simulation of No-Load Characteristics for ORPMPCPA. Based on the design scheme for the ORPMPCPA, the transient field calculation module of finite element analysis platform ANSYS Maxwell2D is used to simulate accurately the dynamic operation process of alternator. A simulation model for the ORPMPCPA with three kinds of combined pole and slot is established, and the magnetic density distribution, magnetic line distribution, and no-load back EMF (electromotive force) waveform are simulated and analyzed for the built ORPMPCPA model. The magnetic density distribution of the ORPMPCPA with three kinds of combined pole and slot is shown in Figure 3. It can be noted that in the three cases, the distribution of main magnetic field is relatively uniform, the maximum magnetic density is located at the stator tooth, and the stator tooth flux density is in the range from 1.35 T to 1.85 T. The magnetic density at the tooth obviously increases with an increase in the slot number, and the magnetic density at the top and bottom of permanent magnet is close to zero. It indicates that the shielding cylinder and the stainless steel sheath used for fixing the rotor exhibit good magnetic isolation effect, and thus the utilization ratio of permanent magnet is improved.

The magnetic field distribution of the ORPMPCPA is very complex, and many factors such as the performances of permanent magnetic material, magnetizing method for poles, geometry of pole shoe, and length of air gap should be considered in the design. However, the magnetic leakage coefficient is a key parameter in the design of permanent magnet alternator and will directly influence the performances of the alternator. The distribution of magnetic flux

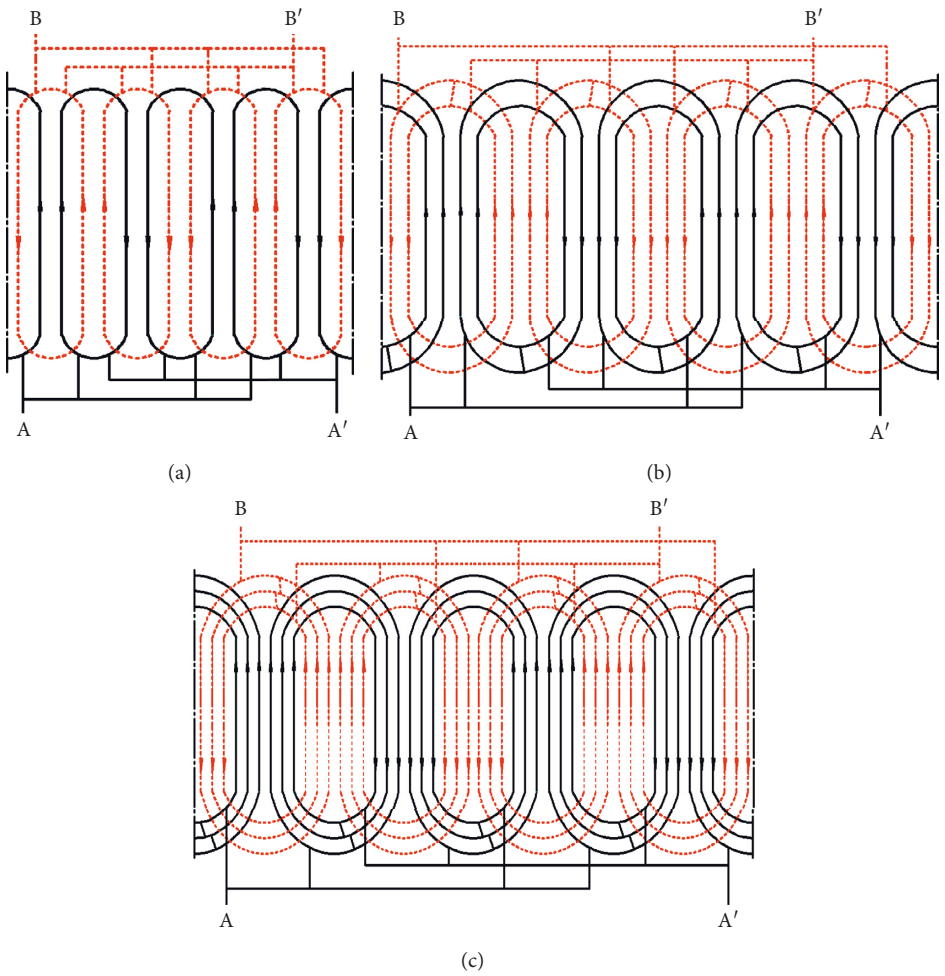

Figure 2: Layout for armature winding of ORPMPCPA with three kinds of combined pole and slot. (a) $q = 2$. (b) $q = 4$. (c) $q = 6$.

lines for the ORPMPCPA, which is obtained under three kinds of combined pole and slot, is shown in Figure 4. It can be noted that for each pole, the magnetic flux lines of the ORPMPCPA symmetrically distribute on both sides of rotor magnetic axis.

The magnetic flux Φ_m is provided for the ORPMPCPA by the permanent magnet, most of which will form the flux linkage with the stator winding, and the corresponding flux is called as the main flux Φ_δ. The remaining flux that does not form the flux linkage with the stator winding is called as the leakage flux Φ_σ. For the ORPMPCPA, a generator excited with the permanent magnet, no-load magnetic leakage flux coefficient σ_0 is also utilized to measure the magnitude of magnetic leakage flux. The calculation method is usually to use the ratio of total magnetic flux Φ_m emitted by permanent magnet under the no-load condition to the main magnetic flux Φ_δ passing through the main magnetic circuit. The calculation formula is as follows:

$$\sigma_0 = \frac{\Phi_m}{\Phi_\delta} = \frac{\Phi_\delta + \Phi_\sigma}{\Phi_\delta}. \tag{7}$$

With the field calculator in the finite element software and based on the magnetic vector potential method, the magnetic leakage flux coefficient can be calculated. It is thought that the relationship between the magnetic vector potential and magnetic flux in a constant magnetic field can be described with the following equation:

$$\Phi = \oint_l A \cdot \mathrm{d}l. \tag{8}$$

Thus, the formula for calculating the magnetic leakage flux coefficient σ_0 can be obtained.

$$\begin{aligned} \sigma_0 &= \frac{\int_{AB} A \cdot \mathrm{d}l + \int_{CD} A \cdot \mathrm{d}l}{\int_{EF} A \cdot \mathrm{d}l} \\ &= \frac{\left|A_A - A_B\right| \cdot l_{AB} + \left|A_C - A_D\right| \cdot l_{CD}}{\left|A_E - A_F\right| \cdot l_{EF}}, \end{aligned} \tag{9}$$

where A_A, A_B, A_C, A_D, A_E, and A_F are, respectively, the magnetic vector potential of points A, B, C, D, E, and F, l_{AB} and l_{CD} are, respectively, the length of lines AB and CD, indicating the region of total flux provided by the permanent magnet, and l_{EF} is the length of arc EF, indicating the region of total flux in the magnetic circuit. The magnetic leakage

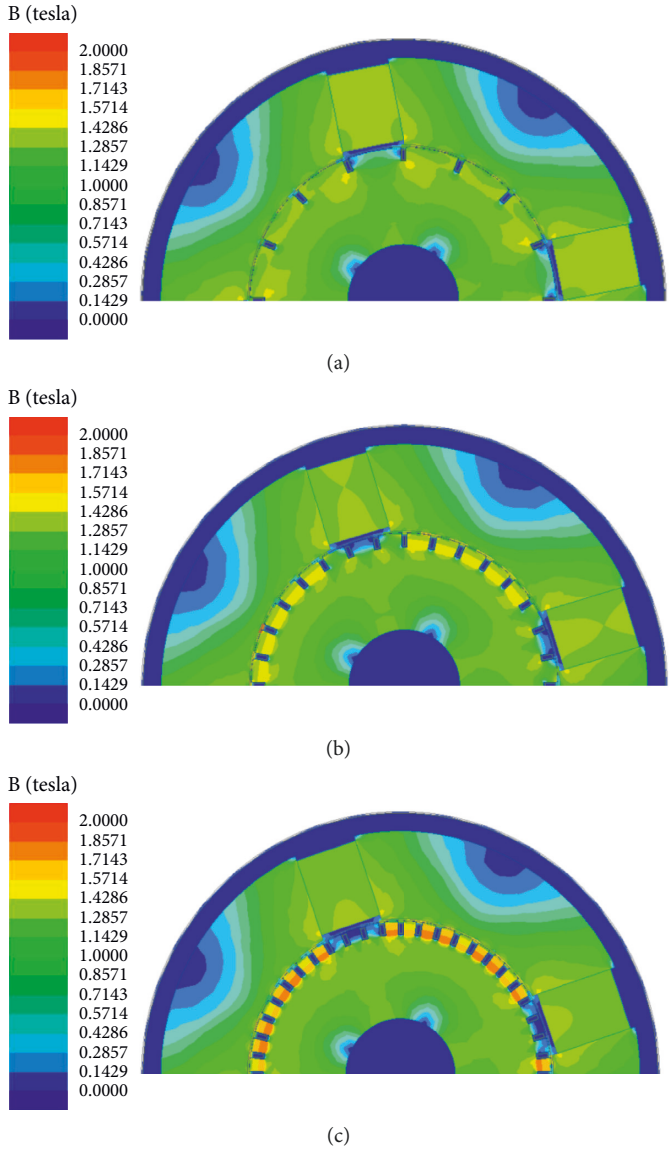

Figure 3: Flux density distribution of ORPMPCPA with three kinds of combined pole and slot. (a) $q = 2$. (b) $q = 4$. (c) $q = 6$.

flux coefficient can be calculated through compiling equation (9) into the field calculator of finite element analysis software. The calculated values of magnetic leakage flux coefficient under three kinds of combined pole and slot are listed in Table 2. The no-load magnetic flux leakage coefficient of the ORPMPCPA is determined to be about 1.08. Obviously, the leakage coefficient is very small, which is beneficial to increase the output voltage of the ORPMPCPA.

The no-load back EMF of the ORPMPCPA is generated through the induction of no-load air gap magnetic flux from the permanent magnet in the armature winding and has a great influence on both output voltage and operation stability of the alternator. The no-load back EMF waveforms of the ORPMPCPA with three kinds of combined pole and slot are shown in Figure 5. It can be seen in the Figure 5 that with an increase of q, the number of turns per phase increases and the value of back EMF also increases. The peak value of back EMF is 2.50 kV at $q = 2$, the peak value of back EMF is 4.50 kV at $q = 4$, and the peak value of back EMF is 6.60 kV at $q = 6$. With the increase of the turns, the output voltage increases under same excitation condition.

However, the increasing trend will drop due to the effect of winding distribution. The slot effect will weaken with the increase in q, and the output waveform is much smoother, which is beneficial to the steady operation of the ORPMPCPA.

3.2. Calculation of Load Parameters for ORPMPCPA. There are many application forms for the CPA. Although the corresponding load types are different, the load parameter shows generally the nonlinear changes with time. According to the operation characteristics of the electromagnetic railgun in the launching process, it can be suggested that if the position of the armature with bearing the gun body varies with time, the armature and the guideway at both ends

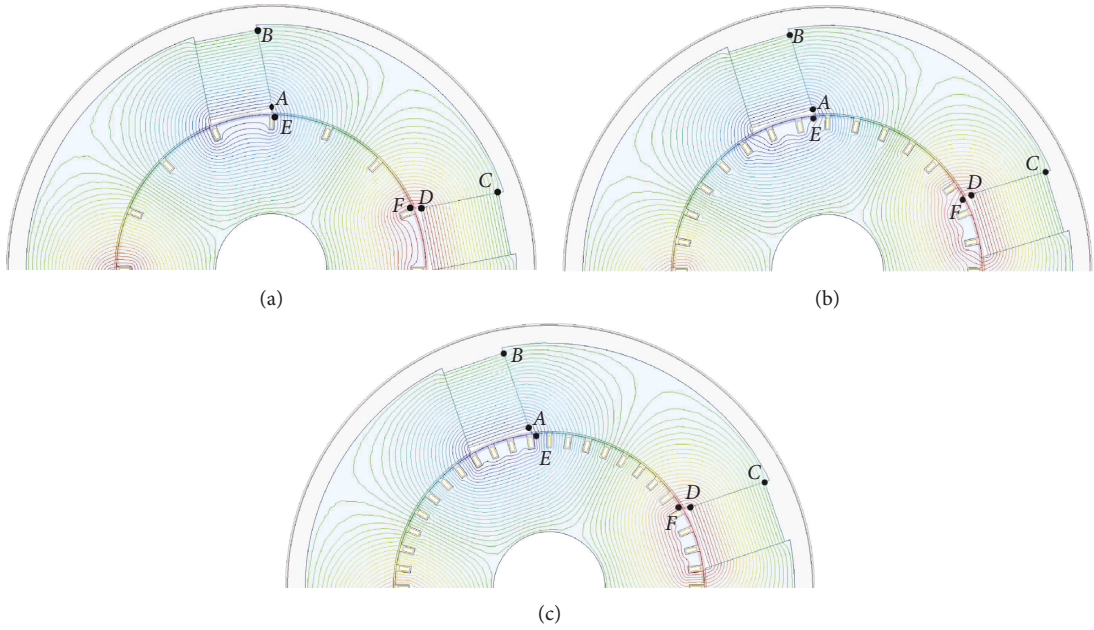

Figure 4: Distribution of magnetic flux lines of ORPMPCPA with three kinds of combined pole and slot. (a) $q = 2$. (b) $q = 4$. (c) $q = 6$.

Table 2: No-load magnetic leakage flux coefficient of the ORPMPCPA under three kinds of combined pole and slot.

Number of slots per phase per pole	2	4	6
Total magnetic flux (Wb)	0.3871	0.3855	0.3831
Main magnetic flux (Wb)	0.3584	0.3569	0.3547
No-load magnetic leakage flux coefficient	1.08	1.08	1.08

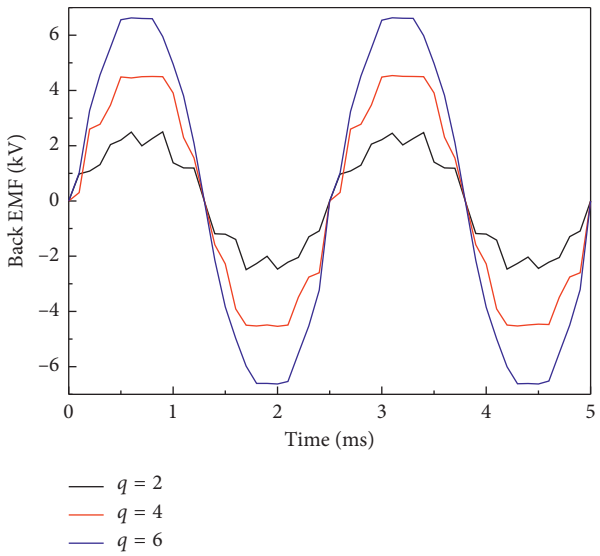

Figure 5: Back EMF waveforms of the ORPMPCPA with three kinds of combined pole and slot.

of the armature can be taken as the load, which can be equivalent to a nonlinear resistance in series with a nonlinear inductance. And the change rule of the load is related to the parameters of the gun body and the current in the circuit.

In the launching process of the electromagnetic railgun, the resultant force acting on the armature and projectile along the axial direction of guideway mainly consists of the Lorenz force to accelerate its operation as well as the air resistance, sliding friction, and ablation resistance to hinder its operation. If the Lorenz force acted on an armature and a projectile is deduced from the aspect of energy conservation and the action from the air resistance, sliding friction resistance and ablation resistance are neglected, and the total energy of electromagnetic railgun can be expressed as follows:

$$W_g = W_m + W_k + W_r = \frac{1}{2}L_r i^2 + \frac{1}{2}mv^2 + \int_0^t i^2 R_r \mathrm{d}t, \quad (10)$$

where W_g is the total energy of the railgun system, W_m is the magnetic energy of the railgun system, W_k is the kinetic energy of projectile and armature, W_r is the thermal energy consumed by the guideway resistor, and m is the total mass of the projectile and armature.

Through solving the derivative of energy to time for the electromagnetic railgun system, the varying ratio of energy can be obtained as follows:

$$\frac{\mathrm{d}W_g}{\mathrm{d}t} = iL_r\frac{\mathrm{d}i}{\mathrm{d}t} + \frac{1}{2}i^2\frac{\mathrm{d}L_r}{\mathrm{d}t} + mv\frac{\mathrm{d}v}{\mathrm{d}t} + i^2R_r. \quad (11)$$

On the other hand, the electrical power transmitted to the electromagnetic railgun by the power supply can be expressed as follows:

$$P = iU = i^2R_r + i^2L'v + iL_r\frac{\mathrm{d}i}{\mathrm{d}t}. \quad (12)$$

Because the electrical power output from the power supply is consistent with the varying rate of energy for the electromagnetic railgun, the acceleration for both the

armature and projectile to move along the guideway is obtained as follows:

$$a = \frac{L' i^2}{2m}. \tag{13}$$

In the accelerating progress of armature along the guideway, the airflow will produce the air resistance to the armature motion. At the same time, the friction resistance is also existent in order to ensure good electric contact between the armature and guideway. In addition, the arc will form in the contact area between the guideway and armature when the current density exceeds the critical value, and thus the resistance caused by the ablation on the guideway forms. The factors influencing the aforementioned resistances are much more and will greatly change with the operating condition. Obviously, it is difficult to perform the accurate calculation for those resistances. Thus, the Lorenz force is usually multiplied with the empirical resistance factor k to represent the total resistance. In this investigation, the value of k is taken as 0.28. The position of armature at different times can be obtained through performing the double integral of acceleration in time. According to the position of armature winding, the values of resistance R_r and inductance L_r for the railgun at the corresponding time can be deduced as follows:

$$R_r = R' \cdot \iint \frac{(1-k)}{2m} L' i^2 \mathrm{d}t + R_0, L_r = L' \cdot \iint \frac{(1-k)}{2m} L' i^2 \mathrm{d}t + L_0, \tag{14}$$

where the resistance gradient R' is 35 $\mu\Omega$/m, the inductance gradient L' is 0.46 μH/m, the initial resistance R_0 is 37 $\mu\Omega$, the initial inductance L_0 is 0.092 μH, and the mass of the armature and projectile m is 160 g.

When the ORPMPCPA drives the railgun system, a single turn coil consisting of the armature and guideway at two sides will generate the magnetic flux. Thus, the back EMF will be produced because the magnetic induction line is cut in the operating process of the armature, which will inhibit the output voltage of the ORPMPCPA and cause the output power to decrease. Obviously, this adverse effect needs to be taken into account. According to the Faraday electromagnetic induction law, the inverse potential produced in the movement process of armature is equal to the variable rate of flux in the circuit. Therefore, the inverse potential at both ends of the armature during the motion of the armature can be described as follows:

$$E = -n\frac{\mathrm{d}\phi}{\mathrm{d}t} = -n\frac{\mathrm{d}(Li)}{\mathrm{d}t} = -n\frac{L'\mathrm{d}xi}{\mathrm{d}t} = -nL' iv, \tag{15}$$

where n is the turn number of coils constructed by the armature and guideway on both sides, i is the current flowing through the armature, and v is the operating speed of armature.

4. Modeling and Simulation Analysis for ORPMPCPA-Driven Railgun System

4.1. Modeling for Railgun System. A collaborative simulation model of the CPA driving railgun system is established to research theoretically the load carrying capacity of the CPA. Because of the magnetic flux compression phenomenon during the discharge of CPA armature winding, the electric inductance of alternator changes instantaneously and the armature reaction is difficult to be expressed with the analytic method. Therefore, in order to consider the influence of change in the electric inductance on the system performances in the discharge process of the CPA, the collaborative simulation with the finite element model for the ORPMPCPA and the circuit model for the railgun system is realized through utilizing the seamless link between the Maxwell2D and Simplorer in the ANSYS software.

When the railgun is fired, the resistance and inductance of guideway as the function of both current and time will change. In the process of establishing the circuit model, it is necessary to achieve the law of change in the railgun parameters according to the firing characteristics of the railgun. Because the component in the ANSYS Simplorer cannot meet the corresponding requirement, the existing models of resistance and inductance are utilized in this investigation, where each step length is, respectively, written into a value to simulate the change of parameters according to the launching rule of the railgun. If the selected step length is enough small, the change rule in the parameters during the launch of the railgun can be approximately simulated. Firstly, the guideway current at each step length is sampled, the resistance and inductance values of railgun at the corresponding time are obtained through the theoretical calculation, and then the obtained values are again brought into the circuit to calculate the next step length so as to obtain the dynamic impedance of guideway. This idea can be also used to calculate the back EMF in the load circuit. Through extracting the armature current and armature speed in real time, the value of back EMF at the corresponding time can be calculated, and thus the change law of back EMF with time is obtained. The simulation model for the whole railgun system is shown in Figure 6.

The circuit model of the railgun can be represented by a variable resistor R_r in series with a variable inductance L_r. The back electromotive force produced by cutting the magnetic line during the high speed operation of armature can be expressed by the DC voltage source E, whose phase is opposite to the output voltage. The internal resistance of two-phase armature winding for the ORPMPCPA can be represented by R_a and R_b, and the leakage inductance at the end of two-phase armature winding can be expressed by L_{ea} and L_{eb}. The two-phase voltages are, respectively, rectified with the full-wave half-controlled rectifying bridge and then are connected in parallel mode to provide the power for the railgun.

The internal resistance of each phase armature winding for the CPA is usually calculated according to the general formula for the DC resistance. However, the inductance at the end of armature winding is complex and will be influenced by many factors. And the windings at the core are shielded so that the inductance of armature winding reduces to a microscale. In this case, the flux linkage at each end of coils turns into a chain to produce the leakage inductance at the end of armature winding. At the same time, the corresponding part of winding will be in the ferromagnetic environment. Because

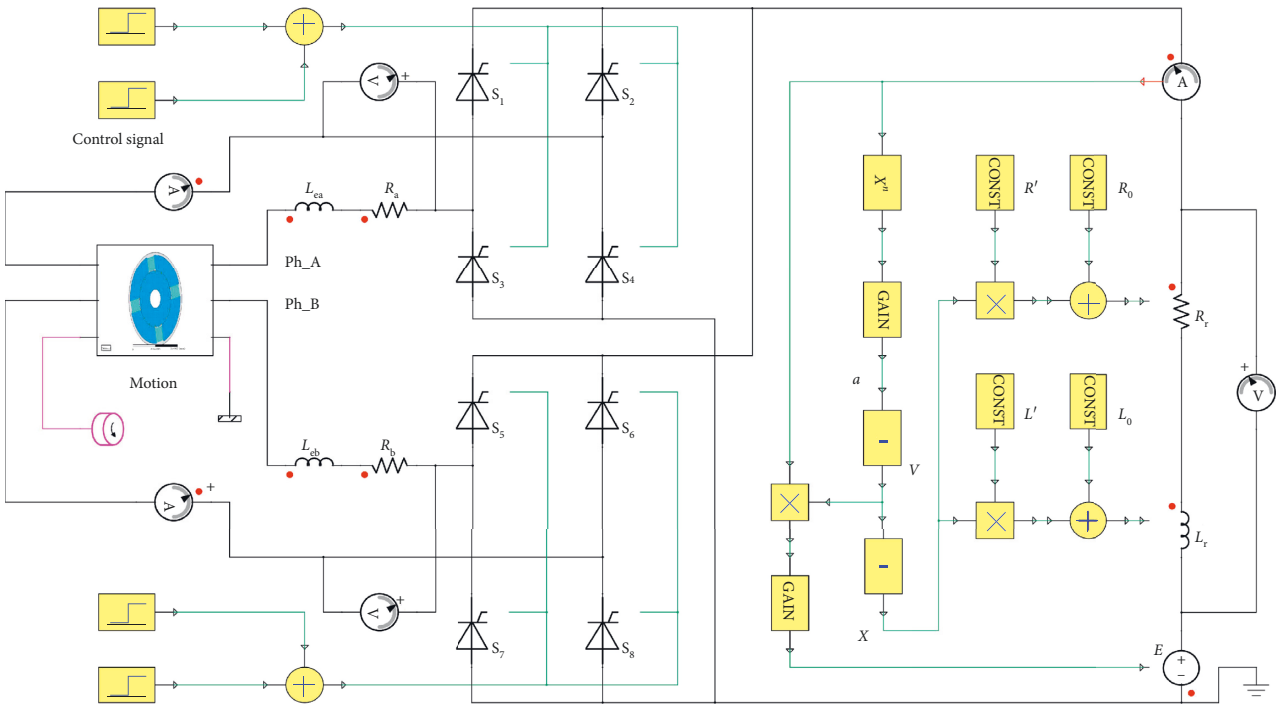

Figure 6: Simulation model for the ORPMPCPA-driven railgun system.

of the magnetic shielding effect, the actual leakage inductance at the end of armature winding is much larger. If no measures are taken, the leakage inductance at the end of armature winding will exceed the inductance in the iron core. It is obvious that the leakage inductance at the end of armature winding must be weakened.

At present, the end of each pole armature winding is covered mainly by a shielded box made of conductive material to shield the leakage inductance at the end. The leakage inductance at the end of armature winding after shielding is almost negligible compared with the inductance at the core. By calculating the shield leakage inductance at the end of wingding, the air gap leakage inductance of each pole winding may be firstly calculated. In order to simplify the calculation, the winding thickness is neglected, and the magnetic permeability of core and the electric conductivity of shielding cylinder are regarded as the infinity. At the same time, the winding current is idealized as the current layer along the outer surface of stator core, and the current of current layer is decomposed into a sequence of harmonic functions based on the Fourier series. In addition, the Laplace polar coordinate magnetic vector equation for the distribution region without the current layer is established, and the separation variable method and magnetic energy product method are used to solve the above problem. Thus, the air gap leakage inductance of each pole winding can be obtained with the following equation:

$$L_\delta = \frac{8\mu_0 l_{\text{ef}} N^2}{\pi} \sum_{n=1,3,5,\ldots}^{\infty} \frac{\sin^2(n\beta/2)}{n^2\beta^2/4} \left(\frac{\delta}{r+n\delta}\right). \tag{16}$$

After the electrical shielding is utilized, the magnetic flux generated at the end of armature winding is also compressed in the air gap. The magnetic flux of armature winding will directly bypass the air gap while does not pass through the rotor core, and the leakage inductance at the end of armature winding is proportional to its end length. Thus, the leakage inductance at the end of each pole winding after introducing the shielding is as follows:

$$L_e = \frac{l_e}{l_{\text{ef}}} L_\delta. \tag{17}$$

In the present investigation, the magnetic permeability of armature winding μ_0 is $4\pi \times 10^{-7}$ H/m, the turns of armature winding in each phase N is 2, 4, and 6, the effective length of stator core l_{ef} is 700 mm, the average equivalent length of armature winding end l_e is 870 mm, the air gap length δ is 1 mm, the outer radius of stator r is 590 mm, and the radian of stator core inner surface held by the armature winding with accounting from the mechanical view β is $\pi/3$. In addition, because the pole number of the ORPMPCPA is 4 and the number of parallel branches is 4, the leakage inductance at the end of each phase winding is 1/4 of leakage inductance at the end of each pole winding. Based on equations (16) and (17), the internal impedance parameters of the ORPMPCPA winding are obtained and are given in Table 3.

4.2. Simulation Analysis. The discharge current waveform of CPA is related to the trigger angle of controller. Considering the magnitude and smoothness of load current waveform and according to the previous control experience for the trigger angle of the ORPMPCPA system, it is suggested that the A phase thyristors S_1~S_4 are controlled to open at 0 ms, the B phase thyristors S_5~S_8 are controlled to open at the

Table 3: Internal impedance parameters of ORPMPCPA winding.

Number of slots per phase per pole	2	4	6
Resistance value of each phase winding (mΩ)	0.063	0.126	0.189
Air gap leakage inductance of each phase winding (nH)	5.12	20.50	46.12
Leakage inductance at the end of each phase winding (nH)	6.36	25.48	57.32

natural commutation point of 0.9375 ms, and both A and B phase thyristors are disconnected simultaneously at 4 ms. Based on the collaborative simulation model for the ORPMPCPA system, the discharge current waveforms of the ORPMPCPA under three kinds of combined pole and slot are obtained and are shown in Figure 7.

It can be seen from Figure 7 that the pulse current waveform obtained with the passive compensation can satisfy the firing requirement of the railgun system. In the launching process of the railgun system, the load impedance increases with an increase in the displacement of armature. The mechanical energy of the rotor is converted into the electric energy, and thus the speed of the rotor reduces. The shielding function of shielding cylinder and the supersaturation state of stator core in the discharging process can cause the decrease of pulse discharge current after reaching the peak value. Under three kinds of combined pole and slot, the discharge current is minimum when the slot number of per phase per pole, q, is 2. Although the very small series turns of each phase can reduce the internal impedance of the CPA, the reduction in the turns of each phase will lead to the low back EMF, and thus the output voltage is not enough. The discharge current is larger when the slot number of per phase per pole is 4 and 6. When the slot number of per pole per equals to 6, the peak output current is slightly higher than that when the slot number of per pole per is 4, while the average output current in the discharging process is smaller than that when the slot number of per pole per is 4. Obviously, the more the turns in each phase winding of the ORPMPCPA is, the higher the output voltage is. However, more turns will cause too large internal impedance of the ORPMPCPA and thus affects the output of pulse current. In addition, higher output voltage will bring great difficulties to the winding insulation and the manufacture of the ORPMPCPA.

According to the principle of passive compensation, the eddy current will be induced in the shielding cylinder due to the change in the armature winding current during the discharge of the ORPMPCPA. Thus, the magnetic flux generated by the stator winding cannot pass through the rotor shielding cylinder and is compressed around the stator winding to reduce the transient inductance of stator winding. Under three kinds of combined pole and slot, when the discharge current of the ORPMPCPA reaches the peak value, the magnetic field distribution of stator is as shown in Figure 8.

It can be noted that the magnetic flux of stator winding can be uniformly compressed at the inner side of shielding

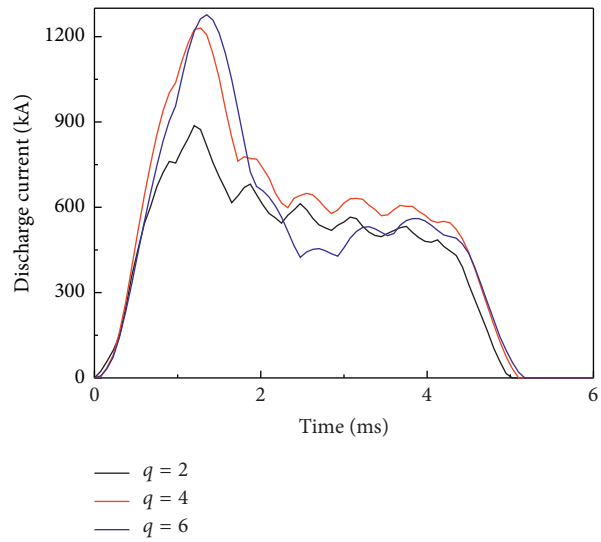

Figure 7: Discharge current waveforms of ORPMPCPA system under three kinds of combined pole and slot.

cylinder through the passive compensation mode. Thus, the magnetoresistance gets increased and the transient inductance of winding gets reduced. The magnetic density of stator core increases gradually with the increase of q, and the stator tooth shows a supersaturating state. Although the supersaturation of stator core will cause a certain attenuation of back EMF, the great magnetoresistance at the saturation will be favorable to the reduction in the transient inductance of winding, and thus the discharge capacity of the CPA will be enhanced. Based on the finite element analysis model, the average values of per phase inductance in the discharge process of armature winding are determined as 1.36 μH, 2.45 μH, and 6.46 μH, respectively, when the slot number of per pole each phase is 2, 4, and 6.

According to the railgun model, the relationship between the armature speed and time under three kinds of combined pole and slot is obtained and is shown in Figure 9. It can be noted from Figure 9 that the armature is the closest to the uniformly accelerated motion when q equals to 2. The acceleration of armature is larger in the initial stage and then tends to be stable when q equals to 4. The fluctuation in the acceleration of armature is relatively larger when q equals to 6. Under three kinds of combined pole and slot, the change trend of acceleration agrees with that of corresponding discharge current waveform. When the armature moves to the end of guideway, the outlet speed of armature is maximum and equals to 2087 m/s at the q value of 4, which can meet the practical requirement of the railgun. In addition, the outlet speed of the armature is slightly small and equals to 1934 m/s at the q value of 6, while the outlet speed of armature is minimum and equals to 1538 m/s at the q value of 2.

The relationship between the armature position and time under three kinds of combined pole and slot is shown in Figure 10. It can be noted that the movement of armature along the guideway gets inconstantly accelerated with the increase of time. The initial position of armature is 0.2 m,

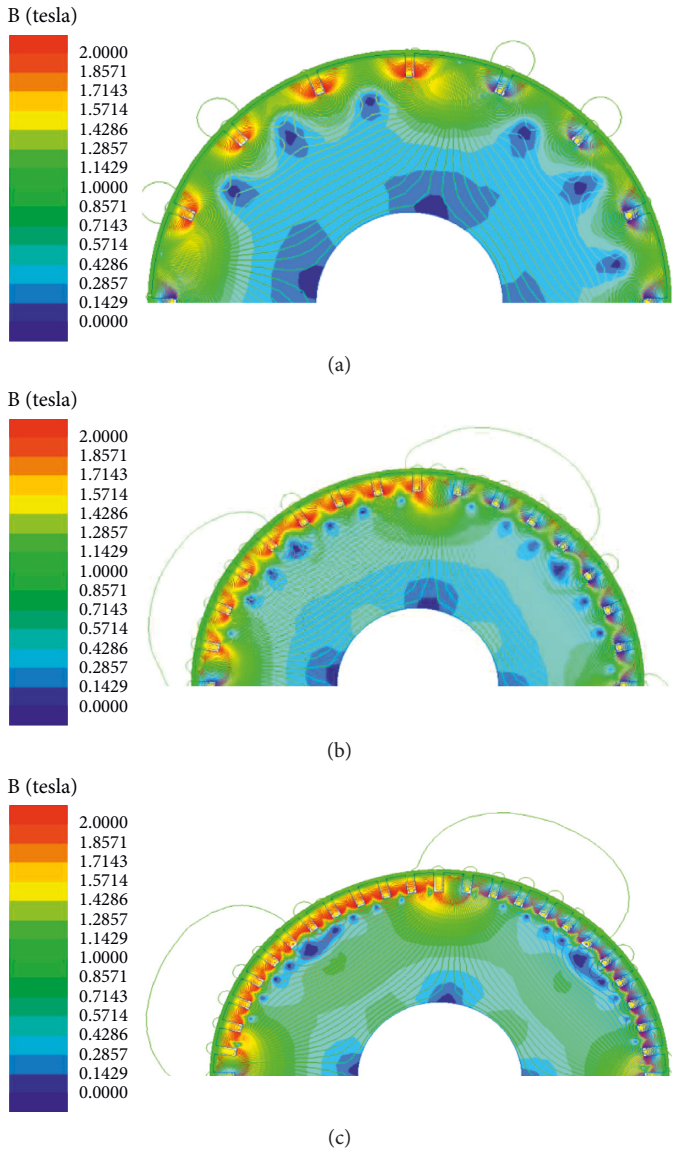

Figure 8: Magnetic field distribution of stator at peak discharge of ORPMPCPA under three kinds of combined pole and slot. (a) $q = 2$. (b) $q = 4$. (c) $q = 6$.

and the overall length of guideway is 4 m, and the armature leaves, respectively, the guideway at 4.5 ms, 3.6 ms, and 3.7 ms when q is 2, 4, and 6. Because the load impedance and inductance are linearly related to the armature position, the varying trend of load impedance with time is same as that of armature position with time. Synthetically considering the no-load characteristics of the ORPMPCPA, output characteristics of the ORPMPCPA, and operating performances of the railgun system, the scheme with the q value of 4 is more appropriate under three kinds of combined pole and slot.

The electromagnetic railgun system is composed of three parts, including the ORPMPCPA, projectile-carrying armature, and two parallel metal guideways. As mentioned, when the projectile-carrying armature moves along the guideway during the launch of the electromagnetic railgun system, the back EMF of armature will generate at both ends of the armature. The relation between the back EMF of the armature and time under three kinds of combined pole and slot is shown in Figure 11. The back EMF of the armature is affected by the armature current and armature speed, and thus the fluctuation in the armature current results in a certain fluctuation in the back EMF of the armature although the armature speed continuously increases. In addition, the greater the current fluctuation is, the more obvious the fluctuation in the back EMF is. When the armature moves to the end of the guideway, the corresponding back EMF of the armature is 0.33 kV, 0.56 kV, and 0.49 kV at the q values of 2, 4, and 6. If the mass and speed of the armature are further increased, the back EMF of the armature will rise and even reach to thousand Volts, and the output of the CPA will be suppressed. At the same time, when the armature leaves the guideway, the excessive terminal voltage of the railgun will cause arc discharge, which will cause great vibration and

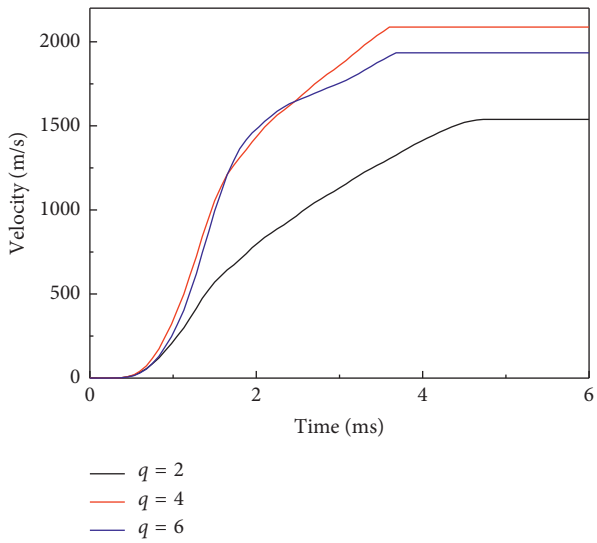

Figure 9: Velocity of armature in ORPMPCPA-driven railgun system under three kinds of combined pole and slot.

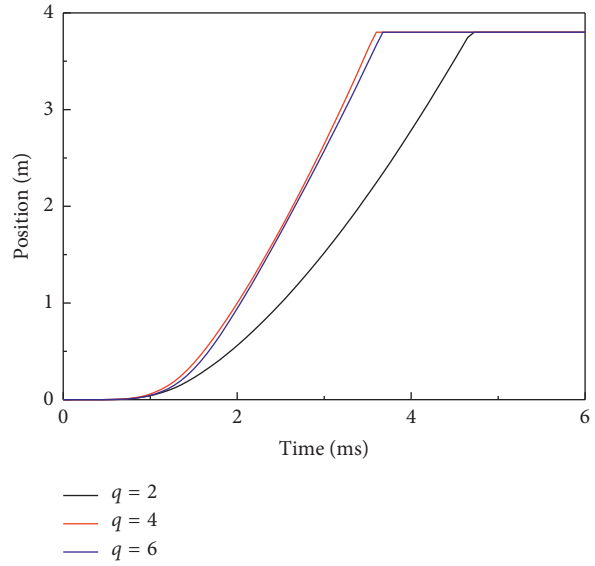

Figure 10: Position of armature in ORPMPCPA-driven railgun system under three kinds of combined pole and slot.

noise and damage the guideway in serious condition. Therefore, the influence of back EMF of the armature on the performances of the ORPMPCPA system cannot be neglected. It can be noted that the magnitudes of back EMF are obviously different in Figures 5 and 11. The difference in the magnitude of back EMF is related to the difference in the generating part of back EMF. The back EMF of the ORPMPCPA in Figure 5 is generated at the pulse power supply side to provide the output voltage for the system, while the back EMF of the armature in Figure 11 is generated at the load side considering the suppression effect on the system voltage. It is obvious that the back EMF of the ORPMPCPA is much larger than the back EMF of the armature.

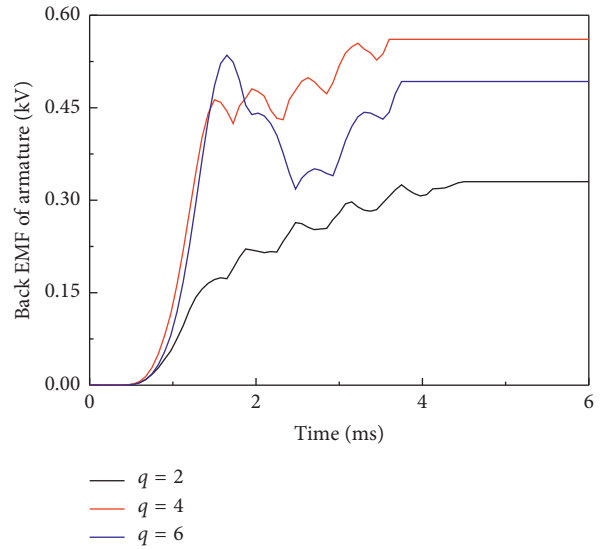

Figure 11: Back EMF of the armature in the ORPMPCPA-driven railgun system under three kinds of combined pole and slot.

5. Conclusions

The designed ORPMPCPA can output strong pulse current in a short time. At the same time, the problems that the winding is difficult to be cooled and fixed during the discharge process of pulsed alternator as well as that the shielding element is easy to deform and needs to be used in conjunction with the reversing device and energy storage flywheel are solved. Based on the calculation of load parameters and the finite element method, a cooperative simulation model for the ORPMPCPA-driven railgun system is established and applied for the simulation of the system. The corresponding simulation results reveal that the compression of armature winding flux can be realized with the passive compensation, the transient inductance of windings can be reduced, and higher power density and better system performances can be achieved with the suitably combined pole and slot. In addition, the existence of back EMF of armature during the launching process of the railgun is clarified. It is obvious that the adverse effect of back EMF of the armature on the operation of the system cannot be ignored.

Data Availability

Both system model parameters and simulation results used to support the findings of this study are included within the article.

Conflicts of Interest

The authors declare that they have no conflicts of interest.

Acknowledgments

The authors gratefully acknowledge the financial support provided by the Natural Science Foundation of China (no. 51774084).

References

[1] A. S. Kulkarni and M. J. Thomas, "Design of a compulsator to drive a railgun," *IEEE Transactions on Plasma Science*, vol. 45, no. 7, pp. 1482–1488, 2017.

[2] X. Xie, K. Yu, C. Ye, Q. You, L. Tang, and H. Zhang, "Design considerations of an air-core pulsed alternator in an electromagnetic railgun system," *IEEE Transactions on Plasma Science*, vol. 43, no. 11, pp. 3895–3900, 2015.

[3] I. R. McNab, "Pulsed power options for large EM launchers," *IEEE Transactions on Plasma Science*, vol. 43, no. 5, pp. 1352–1357, 2015.

[4] S. Wu, W. Zhao, S. Wang, and S. Cui, "Overview of pulsed alternators," *IEEE Transactions on Plasma Science*, vol. 45, no. 7, pp. 1078–1085, 2017.

[5] K. Yu, J. Zhang, X. Xie, S. Yin, and L. Li, "The research of an equivalent load used for testing an air-core pulsed alternator," *IEEE Transactions on Plasma Science*, vol. 47, no. 8, pp. 4189–4195, 2019.

[6] O. Liebfried, S. Hundertmark, and P. Frings, "Inductive pulsed power supply for a railgun artillery system," *IEEE Transactions on Plasma Science*, vol. 47, no. 5, pp. 2550–2555, 2019.

[7] I. R. McNab, "Large-scale pulsed power opportunities and challenges," *IEEE Transactions on Plasma Science*, vol. 42, no. 5, pp. 1118–1127, 2014.

[8] P. Yuan, K. Yu, and C. Ye, "Design and simulation of an active compensated pulsed alternator for the flashlamp load," *IEEE Transactions on Plasma Science*, vol. 41, no. 5, pp. 1225–1230, 2013.

[9] C. Chakraborty, S. Basak, and Y. T. Rao, "Synchronous generator with embedded brushless synchronous exciter," *IEEE Transactions on Energy Conversion*, vol. 34, no. 3, pp. 1242–1254, 2019.

[10] S. Basak, C. Chakraborty, and B. C. Pal, "A new configuration of dual stator induction generator employing series and shunt capacitors," *IEEE Transactions on Energy Conversion*, vol. 33, no. 2, pp. 762–772, 2018.

[11] J. K. Li, J. Q. Wang, Y. Xu et al., "Research on the transient characteristics of microgrid with pulsed load," *Mathematical Problems in Engineering*, vol. 2015, Article ID 105387, 15 pages, 2015.

[12] C. Ye, W. Li, F. Xiong, X. Liang, and Z. Zhu, "Study of operation principle of a novel brushless self-excited air-core compensated pulsed alternator," *IEEE Transactions on Plasma Science*, vol. 47, no. 5, pp. 2362–2368, 2019.

[13] J. Li, X. Yan, L. Lv, L. Tan, J. Tian, and J. Lou, "Pulsed power regulation in selective passively compensated pulsed alternator," *IEEE Transactions on Magnetics*, vol. 48, no. 11, pp. 3875–3878, 2012.

[14] Q. Zhang, S. Wu, C. Yu, S. Cui, and L. Song, "Design of a model-scale air-core compulsator," *IEEE Transactions on Plasma Science*, vol. 39, no. 1, pp. 346–353, 2011.

[15] W. Zhao, X. Wang, S. Wu, S. Cui, C. Gerada, and H. Yan, "Research on the compensation matching design and output performance for two-axis-compensated compulsators," *IEEE Transactions on Plasma Science*, vol. 47, no. 5, pp. 2445–2451, 2019.

[16] W. Li, H. Qiu, X. Zhang, J. Cao, S. Zhang, and R. Yi, "Influence of rotor-sleeve electromagnetic characteristics on high-speed permanent-magnet generator," *IEEE Transactions on Industrial Electronics*, vol. 61, no. 6, pp. 3030–3037, 2014.

[17] K. Yu, J. Yao, X. Xie, F. Zhang, and P. Tang, "3-D FEM analysis on electromagnetic characteristics of an air-core pulsed alternator," *IEEE Transactions on Plasma Science*, vol. 45, no. 7, pp. 1257–1262, 2017.

[18] L. Tang and K. Yu, "Magnetic and conductive shielding for air-core pulsed alternators in railgun systems," *IEEJ Transactions on Electrical and Electronic Engineering*, vol. 11, no. 5, pp. 665–670, 2016.

[19] L. Tang, K. Yu, X. Xie, and H. Zhang, "Discharge process of the multiphase air-core compulsator-based railgun systems," *IEEE Transactions on Plasma Science*, vol. 44, no. 3, pp. 273–280, 2016.

[20] L. Gao, Z. X. Li, and B. M. Li, "The modeling and calculation on an air-core passive compulsator," *IEEE Transactions on Plasma Science*, vol. 43, no. 3, pp. 864–868, 2015.

[21] X. Li, S. Cui, and L. Song, "High-efficiency control strategy of an air-core pulsed alternator pair," *IEEE Transactions on Plasma Science*, vol. 45, no. 12, pp. 3342–3348, 2017.

[22] Y. T. Rao, C. Chakraborty, and S. Basak, "Brushless induction excited synchronous generator with induction machine operating in plugging mode," *IEEE Transactions on Industry Applications*, vol. 54, no. 6, pp. 5748–5759, 2018.

[23] S. Basak and C. Chakraborty, "A new optimal current control technique for dual stator winding induction generator," *IEEE Journal of Emerging and Selected Topics in Power Electronics*, vol. 5, no. 2, pp. 820–832, 2017.

[24] J. K. Noland, F. Evestedt, and U. Lundin, "Active current sharing control method for rotating thyristor rectifiers on brushless dual-star exciters," *IEEE Transactions on Energy Conversion*, vol. 33, no. 2, pp. 893–896, 2018.